Comparison of Finite Volume Flux Vector Splittings for the Euler Equations

W. Kyle Anderson* and James L. Thomas*
NASA Langley Research Center, Hampton, Virginia
and
Bram Van Leer*
Delft University of Technology, Delft, the Netherlands

A flux-splitting method in generalized coordinates has been developed and applied to quasi-one-dimensional transonic flow in a nozzle and two-dimensional subsonic, transonic, and supersonic flow over airfoils. Computational results using the Steger-Warming and Van Leer flux splittings are compared. Discussed are several advantages of a MUSCL-type approach (differencing followed by flux splitting) over a standard flux differencing approach (flux splitting followed by differencing). With an approximately factored implicit scheme, spectral radii of 0.978-0.930 for a series of airfoil computations are obtained, generally decreasing as a larger portion of the flow becomes supersonic. The Van Leer splitting leads to higher convergence rates and a sharper representation of shocks, with at most two (but more often, one) zones in the shock transition. The second-order accurate one-sided-difference model is extended to a third-order upwind-biased model with a small additional computational effort. The results for both the second- and third-order schemes agree closely in overall features to a widely used central difference scheme, although the shocks are resolved more accurately with the flux splitting approach.

Nomenclature

a = speed of sound
e = total energy per unit volume
F,G = fluxes of mass, momentum, and energy
p = pressure
Q = conserved variables
t = time
u,v = Cartesian velocities
x,y = Cartesian coordinates
γ = ratio of specific heats, = 1.4
ρ = density

Superscripts

n = time level
$\pm$ = positive and negative flux contributions; also forward and backward spatial differencing or extrapolation

Introduction

IN the solution of hyperbolic equations such as the time-dependent Euler equations, the theory of characteristics is crucial in determining the directions of the signal propagation. The information gained from the characteristic theory, for example, has been very useful in the development of boundary conditions that are both physically correct and mathematically well posed. Recently, much interest has been generated in the development of computational methods for the Euler equations that model the underlying physics, as dictated by characteristic theory, at each grid point. These methods can be classified, in general, as upwind methods and have the advantage of being naturally dissipative. Separate spatial dissipation terms, such as those generally required in a central difference method to overcome oscillations or instabilities arising in regions of strongly varying gradients, need not be added.

Received Dec. 20, 1984; presented as Paper 85-0122 at the AIAA 23rd Aerospace Sciences Meeting, Reno, NV, Jan. 14-17, 1985; revision submitted Oct. 10, 1985.

*Research Scientist. Member AIAA.

Many of these methods are applied to the nonconservative form of the equations and consequently require the use of shock-fitting techniques to obtain the correct location and strength of shocks in transonic flows. Use of the conservation law form allows the shock waves to be captured as weak solutions to the governing equations and circumvents the difficulty in applying shock-fitting techniques to arbitrary flows. Both flux difference and flux vector splitting methods can be applied to the conservation law form; only flux vector splitting or, in brief, flux splitting, is considered in the present work.

Steger and Warming,[1] making use of similarity transformations and the homogeneity property of the Euler equations, split the flux vector into forward and backward contributions by splitting the eigenvalues of the Jacobian matrix

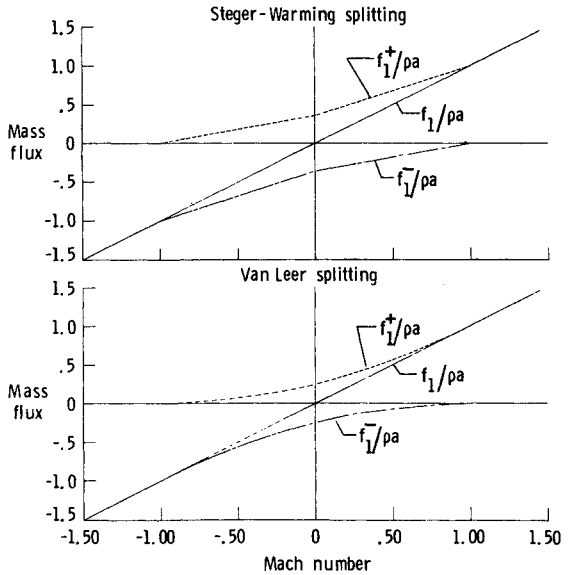

Fig. 1 Variation of mass flux with Mach number for Steger-Warming and Van Leer splittings.

of the full flux into non-negative and nonpositive groups. The split flux contributions are then spatially differenced according to one-sided upwind discretizations. The Steger-Warming splitting has been widely used, with varying degrees of success, and has also been implemented in generalized coordinates.[2] Its main shortcoming is that the forward and backward fluxes are not differentiable when an eigenvalue changes sign, such as occurs at sonic points; this leads to the occurrence of small glitches or oscillations in these regions. Van Leer[3] introduced an alternate flux splitting with continuously differentiable flux contributions that lead to smoother solutions at sonic points. In addition, the splitting is designed so that the shock structures can be realized with no more than two interior zones.

The use of this alternate splitting method in computing two-dimensional flow about airfoils in a general coordinate system has been very limited. The implementation of Van Leer's flux splitting in generalized coordinates and a comparison of the results with those obtained with the Steger-Warming splitting are the main purposes of this investigation.

Flux Splitting

Cartesian Coordinates

The two-dimensional Euler equations expressed in Cartesian coordinates and conservation form are

$$\frac{\partial Q}{\partial t}+\frac{\partial F}{\partial x}+\frac{\partial G}{\partial y}=0 \tag{1}$$

where

$$Q=\begin{Bmatrix}\rho\\ \rho u\\ \rho v\\ e\end{Bmatrix},\quad F=\begin{Bmatrix}\rho u\\ \rho uu+p\\ \rho uv\\ u(e+p)\end{Bmatrix},\quad G=\begin{Bmatrix}\rho v\\ \rho uv\\ \rho vv+p\\ v(e+p)\end{Bmatrix} \tag{2}$$

with the equation of state given by

$$p=(\gamma-1)\left[e-\frac{\rho(u^2+v^2)}{2}\right] \tag{3}$$

For the current study, two methods of splitting the flux vectors are considered, the first of which was presented by Steger and Warming in Ref. 1. In this method, the flux vector F, for example, can be expressed in terms of the eigenvalues λ_i of its Jacobian matrix A as

$$F=\frac{\rho}{2\gamma}\begin{Bmatrix}2(\gamma-1)\lambda_1+\lambda_3+\lambda_4\\ 2(\gamma-1)\lambda_1 u+\lambda_3(u+a)+\lambda_4(u-a)\\ 2(\gamma-1)\lambda_1 v+\lambda_3 v+\lambda_4 v\\ (\gamma-1)\lambda_1(u^2+v^2)+W\\ \quad+(\lambda_3/2)[(u+a)^2+v^2]\\ \quad+(\lambda_4/2)[(u-a)^2+v^2]\end{Bmatrix} \tag{4}$$

where

$$W=\frac{(3-\gamma)(\lambda_3+\lambda_4)a^2}{2(\gamma-1)}$$

and

$$\lambda_1=u,\quad \lambda_3=u+a,\quad \lambda_4=u-a \tag{5}$$

The forward and backward flux vectors F^+ and F^-, for example, are formed from Eq. (4) by inserting $\lambda_i=\lambda_i^+$ and $\lambda_i=\lambda_i^-$, respectively, where $\lambda_i^\pm=(\lambda_i\pm|\lambda_i|)/2$. It should be noted that for supersonic and sonic flow, i.e., $|M_x|=|u/a|\geq 1$,

$$F^+=F,\quad F^-=0\quad \text{for } M_x\geq 1$$

$$F^-=F,\quad F^+=0\quad \text{for } M_x\leq -1 \tag{6}$$

The fluxes split as above are not continuously differentiable at zeros of the eigenvalues (i.e., sonic and stagnation points). In Fig. 1a, the mass flux f_1 from Eq. (4), nondimensionalized by division through by ρa, is shown as a function of the Mach number. The gradient discontinuities in the flux are evident as the eigenvalues pass through zero. The lack of differentiability of the split fluxes has been shown in previous studies to cause small oscillations or glitches at sonic points.[1,2,4] These oscillations can be reduced by the introduction of a small parameter ϵ to the eigenvalue-switching technique[2,4] and by redefining λ_i^+ and λ_i^- as

$$\lambda_i^\pm=\frac{\lambda_i\pm(\lambda_i^2+\epsilon^2)^{1/2}}{2} \tag{7}$$

These functions of λ_i are represented by hyperbolas of height $\epsilon/2$ at $\lambda_i=0$. This alternate approach allows a smooth transition of the solution through the sonic point. Note, however, that Eq. (6) is no longer valid. A form similar to Eq. (4) is obtained for the split-flux representation of G in terms of the eigenvalues of its Jacobian matrix B, which are v, $v+a$, and $v-a$.

Correspondingly, for the splitting suggested by Van Leer, $F^\pm$ is given in terms of the local one-dimensional Mach number $M_x\equiv u/a$. For supersonic flow, i.e., $|M_x|\geq 1$, we have

$$F^+=F,\quad F^-=0\quad \text{for } M_x\leq 1$$

$$F^+=0,\quad F^-=F\quad \text{for } M_x\leq -1 \tag{8}$$

and for subsonic flow $|M_x|<1$

$$F^\pm=\begin{Bmatrix}f_1^\pm\\ f_1^\pm[(\gamma-1)u\pm 2a]/\gamma\\ f_1^\pm v\\ f_1^\pm[\{(\gamma-1)u\pm 2a\}^2/\{2(\gamma^2-1)\}+v^2/2]\end{Bmatrix} \tag{9}$$

where

$$f_1^\pm=\pm\rho a[\tfrac{1}{2}(M_x\pm 1)]^2$$

In Fig. 1b, the nondimensionalized mass flux from Eq. (9) is shown as a function of the Mach number. The split flux is continuously differentiable at the sonic and stagnation points; the improvement in comparison to the Steger-Warming splitting is apparent. The splitting for G is obtained similarly in terms of the local one-dimensional Mach number $M_y\equiv v/a$.

Extension to Generalized Coordinates

For the analysis of the flow over airfoils, it is advantageous to construct generalized (body-fitted) coordinate systems of the type

$$\xi=\xi(x,y),\quad \eta=\eta(x,y) \tag{10}$$

where, in the present work, the transformation is chosen so that the grid spacing in the computational domain is uniform and of unit length; i.e., $\Delta\xi=1$ and $\Delta\eta=1$. In the discussion

that follows, the superscript ($\hat{}$) indicates variables in the generalized coordinates, while an overbar ($\bar{}$) indicates variables in a locally Cartesian system. If no superscript is used, Cartesian coordinates are assumed. The strong conservation form of the Euler equations in generalized coordinates is

$$\frac{\partial \hat{Q}}{\partial t}+\frac{\partial \hat{F}}{\partial \xi}+\frac{\partial \hat{G}}{\partial \eta}=0 \tag{11}$$

where

$$\hat{Q}=Q/J, \quad \hat{F}=(\xi_x F+\xi_y G)/J$$

$$\hat{G}=(\eta_x F+\eta_y G)/J \tag{12}$$

The Jacobian of the transformation, J, physically corresponds to the inverse of the cell volume. The vectors (grad ξ)/J and (grad η)/J correspond to directed areas of cell interfaces in the ξ and η directions, respectively.

For the purpose of determining a generalized splitting for $\hat{F}$, only the derivatives in the ξ and t directions are considered, while the η derivatives are treated as source terms. Conversely, when splitting $\hat{G}$, the ξ derivatives are treated as source terms. For determining the splitting of $\hat{F}$, Eq. (11) is transformed by a local rotation matrix T given by

$$T=\begin{bmatrix} 1 & 0 & 0 & 0 \\ 0 & \cos\theta & \sin\theta & 0 \\ 0 & -\sin\theta & \cos\theta & 0 \\ 0 & 0 & 0 & 1 \end{bmatrix} \tag{13}$$

where

$$\cos\theta=\xi_x/|\text{grad }\xi|$$

$$\sin\theta=\xi_y/|\text{grad }\xi|$$

Multiplication of Eq. (11) with the matrix T then yields

$$\bar{Q}_t+\bar{F}_\xi=-T\hat{G}_\eta+T_t\hat{Q}+T_\xi\hat{F} \tag{14}$$

where

$$\bar{Q}=T\hat{Q}=\frac{1}{J}\begin{Bmatrix} \rho \\ \rho\bar{u} \\ \rho\bar{v} \\ e \end{Bmatrix} \tag{15}$$

$$\bar{F}=T\hat{F}=\frac{|\text{grad }\xi|}{J}\begin{Bmatrix} \rho\bar{u} \\ \rho\bar{u}\bar{u}+p \\ \rho\bar{u}\bar{v} \\ (e+p)\bar{u} \end{Bmatrix} \tag{16}$$

The rotated velocity component $\bar{u}$ is the velocity normal to a line of constant ξ representing the scaled contravariant velocity component and $\bar{v}$ is normal to $\bar{u}$,

$$\bar{u}=(\xi_x u+\xi_y v)/|\text{grad }\xi|$$

$$\bar{v}=(-\xi_y u+\xi_x v)/|\text{grad }\xi|$$

The transformed flux $\bar{F}$ is of the same functional form as the Cartesian flux vector and thus can be split according to any splitting developed for Cartesian coordinates. Therefore, the equations given in the previous section for both the Steger-Warming and the Van Leer splittings can be used to split the flux vector $\bar{F}$ after replacing the Cartesian velocity components u and v by the rotated velocity components $\bar{u}$ and $\bar{v}$. Applying the rotation T to Eq. (11) simply allows us to split the flux vector in a one-dimensional fashion, along a coordinate axis perpendicular to the cell interface. After splitting $\bar{F}$, the appropriate splitting for $\hat{F}$ is determined by applying the inverse transformation matrix T^{-1} to Eq. (14), leading to

$$\hat{Q}_t+(\hat{F}^+ +\hat{F}^-)_\xi+\hat{G}_\eta=0 \tag{17}$$

with

$$\hat{F}^+=T^{-1}\bar{F}^+, \quad \hat{F}^-=T^{-1}\bar{F}^- \tag{18}$$

Note that the inverse transformation restores the original form of the equations, i.e., no additional source terms arise and the form of $\hat{G}$ is unaffected. This allows a splitting of $\hat{G}$ similar to the splitting of $\hat{F}$ shown above. Carried out with the Steger-Warming splitting, the above procedure recovers identically the generalized splitting given in Ref. 1.

Spatial Differencing

In numerical solutions to the flux-split Euler equations, the spatial derivatives of F^+ and F^-, for example, can be approximated with backward and forward difference operators, respectively, denoted herein as δ_x^- and δ_x^+. The standard first- and second-order backward differences on a uniformly spaced grid are given by

$$\delta_x^- F_i^+=\frac{1}{\Delta x}(F_i^+-F_{i-1}^+)=\left(\frac{\partial F^+}{\partial x}\right)_i+\mathcal{O}(\Delta x)$$

$$\delta_x^- F_i^+=\frac{1}{\Delta x}\left(\frac{3}{2}F_i^+-2F_{i-1}^+ +\frac{1}{2}F_{i-2}^+\right)=\left(\frac{\partial F^+}{\partial x}\right)_i+\mathcal{O}[(\Delta x)^2]$$

These formulas can be combined by writing δ_x as the sum of a first-order term and a correction for second-order accuracy

$$\delta_x^- F_i^+=\frac{1}{\Delta x}(F_i^+-F_{i-1}^+)+\frac{\phi_i^-}{2\Delta x}(F_i^+-F_{i-1}^+)-\frac{\phi_{i-1}^-}{2\Delta x}(F_{i-1}^+-F_{i-2}^+) \tag{19}$$

The order of accuracy of the approximation is governed by the value of the switch ϕ^-: second-order accuracy for $\phi^-=1$, first order for $\phi^-=0$. Spatial variation of ϕ^- allows conservative switching between the second- and first-order formulas, which is generally required to eliminate oscillations in regions where the solution is discontinuous, such as shock waves. The switching function ϕ^- is called a limiter, since it serves to limit the second-order term in Eq. (19). Equation (19) can also be written as

$$\delta_x^- F^+=(F_{i+\frac{1}{2}}^+-F_{i-\frac{1}{2}}^+)/\Delta x$$

with

$$F_{i+\frac{1}{2}}^+=F_i^+ +\phi_i^-(F_i^+-F_{i-1}^+)/2$$

In other words, after having obtained F^+ at all nodal points, its value at cell interfaces is determined by forward extrapolation.

An alternative treatment is to first extrapolate nodal point values of Q toward the interfaces and then obtain F^+ at the interfaces. This leads to the following approximation of $\partial F/\partial x$:

$$\delta_x F_i=\frac{1}{\Delta x}[F^+(Q_{i+\frac{1}{2}}^-)-F^+(Q_{i-\frac{1}{2}}^-) +F^-(Q_{i+\frac{1}{2}}^+)-F^-(Q_{i-\frac{1}{2}}^+)] \tag{20}$$

where the notation $F^{\pm}(Q^{\mp})$ denotes $F^{\pm}$ evaluated at $Q^{\mp}$, and

$$Q^{-}_{i+\frac{1}{2}} = Q_i + \phi_i^{-}(Q_i - Q_{i-1})/2 \tag{21}$$

$$Q^{+}_{i+\frac{1}{2}} = Q_{i+1} - \phi^{+}_{i+1}(Q_{i+2} - Q_{i+1})/2 \tag{22}$$

We shall call this the MUSCL (monotone upstream-centered scheme for conservation laws) approach, after the first code incorporating such differencing.[5] As before, the first- and second-order approximations correspond to $\phi^{\pm}=0$ and $\phi^{\pm}=1$, respectively; flux limiting is implemented through a spatial variation of $\phi^{\pm}$ similar to that associated with Eq. (19).

The computational results presented in the next section indicate that MUSCL-type differencing [Eq. (20)] is clearly superior to standard flux differencing [Eq. (19)]. The advantages of the MUSCL approach accrue for several reasons. The fluxes are split according to the local cell interface Mach number, whereas in the flux differencing approach the splitting depends on the Mach numbers in various cell centers. Also, as noted in Ref. 6, the split fluxes are generally less differentiable than the conserved variables when transitioning through sonic and stagnation points. This is particularly true for the Steger-Warming fluxes that, unlike the Van Leer fluxes, are not even once differentiable. Additionally, the MUSCL approach is advantageous in extensions to two and three dimensions in curvilinear coordinates, as an unambiguous choice for the metric factors in the normal fluxes can be made.

Computational results comparing the effects of spatial differencing approximations for a one-dimensional nozzle with transonic flow are presented below. The Mach number variation along the converging-diverging nozzle test problem used in Ref. 4 is shown in Fig. 2. Figure 2a shows results using second-order split-flux differencing [Eq. (19)] with the Steger-Warming flux splitting; Fig. 2b shows the corresponding result with the Van Leer flux splitting. As expected, the smoother variation of the split fluxes with the Van Leer splitting has eliminated the glitch evident at the sonic point with the Steger-Warming splitting. A noticeable drawback to both solutions is that overshoots in the Mach number are obtained just upstream of the shock. Although not shown, the density and pressure variations display similar overshoots and undershoots in the shock region. Figure 2c shows the effect of using Eq. (7) with $\epsilon=0.04$ rather than $\epsilon=0.0$ as the eigenvalue switch in the Steger-Warming fluxes. As can be seen, the glitch at the sonic point has been successfully eliminated, while the shock region is virtually unaffected. Although not shown , the use of a flux limiter resulted in the elimination of the overshoots in the shock region, while not degrading the accuracy of the solution in the smooth region of the flow.

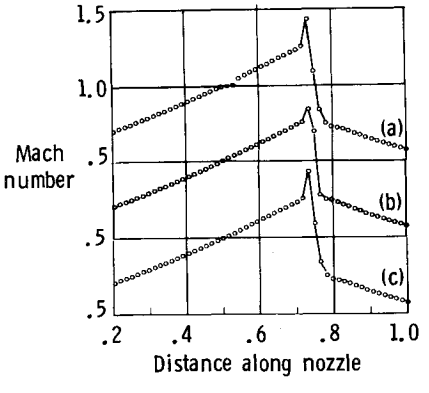

Fig. 2 Mach number distribution along a one-dimensional nozzle using split-flux differencing: a) Steger-Warming, $\epsilon=0$; b) Van Leer; c) Steger-Warming, $\epsilon=0.04$.

Second-order results obtained with MUSCL-type differencing [Eq. (20)] are shown in Fig. 3a for the Steger-Warming splitting with $\epsilon=0$ and in Fig. 3b for the Van Leer splitting. As can be seen, in either solution the oscillations in the shock region are absent, although no flux limiting has been employed. This is an unexpected benefit of MUSCL-type differencing, when incorporated in a fully one-sided scheme. The state quantity that jumps the most across the shock, i.e., the Riemann invariant associated with the characteristic speed that changes sign, is not differenced across the shock (this is easily checked on the basis of Burger's equation). The other quantities are, but carry much smaller jumps if the shock is not too strong. The result is a monotone profile for weak shocks.

The Van Leer splitting leads to a sharper representation of the shock than the Steger-Warming splitting. Note, however, that the Steger-Warming fluxes, although used with zero smoothing parameter, no longer leads to glitches in the solution as it passes through the sonic points. Several other transonic cases were investigated and, in each one, results similar to those shown above were obtained.

Solution Algorithm

After flux splitting, the Euler equations in generalized coordinates are given by

$$\frac{\partial \hat{Q}}{\partial t} + \frac{\partial \hat{F}^{+}}{\partial \xi} + \frac{\partial \hat{F}^{-}}{\partial \xi} + \frac{\partial \hat{G}^{+}}{\partial \eta} + \frac{\partial \hat{G}^{-}}{\partial \eta} = 0 \tag{23}$$

The method of solution is the approximately factored Beam-Warming implicit algorithm[7] given in delta form by

$$\left[I + \Delta t\left(\delta_{\xi}^{-}\frac{\partial \hat{F}^{+}}{\partial \hat{Q}} + \delta_{\xi}^{+}\frac{\partial \hat{F}^{-}}{\partial \hat{Q}}\right)\right]^{n} *$$

$$\left[I + \Delta t\left(\delta_{\eta}^{-}\frac{\partial \hat{G}^{+}}{\partial \hat{Q}} + \delta_{\eta}^{+}\frac{\partial \hat{G}^{-}}{\partial \hat{Q}}\right)\right]^{n} \Delta \hat{Q}_{i,j}$$

$$= -\Delta t[\delta_{\xi}^{-}\hat{F}^{+} + \delta_{\xi}^{+}\hat{F}^{-} + \delta_{\eta}^{-}\hat{G}^{+} + \delta_{\eta}^{+}\hat{G}^{-}]^{n}_{i,j} \tag{24}$$

where $\Delta Q = Q^{n+1} - Q^{n}$. The spatial derivatives are approximated by the MUSCL-type differencing described previously and are implemented in what is commonly referred to as a finite volume formulation. The split-flux differencing in the ξ direction, for example, can be written as

$$\delta_{\xi}^{\mp}\hat{F}^{\pm}_{i,j} = [\hat{F}^{\pm}(Q^{\mp}_{i+\frac{1}{2},j}, M_{i+\frac{1}{2},j}) - \hat{F}^{\pm}(Q^{\mp}_{i-\frac{1}{2},j}, M_{i-\frac{1}{2},j})] \tag{25}$$

The term M represents geometric terms involved in the transformation to generalized coordinates, evaluated at the cell interface locations where the flux values are needed. The values of $Q^{\pm}_{i+\frac{1}{2},j}$ are determined as in the one-dimensional

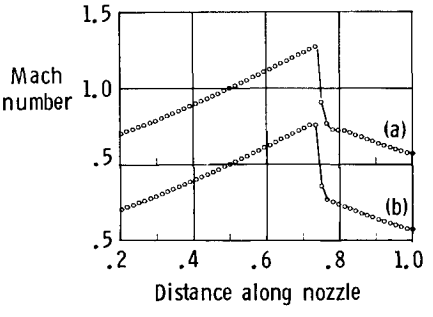

Fig. 3 Mach number distribution along a one-dimensional nozzle using MUSCL-type differencing: a) Steger-Warming; b) Van Leer.

case

$$Q^{-}_{i+\frac{1}{2},j} = Q_{i,j} + \phi^{-}_{i,j}(Q_{i,j} - Q_{i-1,j})/2 \tag{26}$$

$$Q^{+}_{i+\frac{1}{2},j} = Q_{i+1,j} - \phi^{+}_{i+1,j}(Q_{i+2,j} - Q_{i+1,j})/2 \tag{27}$$

Since fluxes and geometric terms are evaluated only at cell interfaces, the above MUSCL-type finite volume formulation leads to a vanishing right-hand side of Eq. (24) for freestream conditions, in contrast to the standard flux-differencing formulation.[2]

First-order upwind differencing is used on the left-hand side of Eq. (24), yielding a block-tridiagonal structure for the implicit equations. Note that the true Jacobians arising from the time linearization of $\hat{F}$ and $\hat{G}$ are used in the results presented below. Appproximations to these matrices that are simpler to form have been used previously, but lead to an explicit-type stability limit for Δt.[8] Since upwind spatial differencing is used, explicit artificial dissipation is not required and hence not used.

The boundary conditions for the airfoil solutions presented subsequently are applied explicitly. On the body, the normal velocity is set to zero and the pressure is determined from the normal momentum equation. The tangential velocity on the surface, needed to compute the normal pressure derivative, is determined by extrapolation from the interior. The density on the surface, likewise needed, is determined by forcing the normal entropy derivative to be zero.

The boundary conditions in the far field with subsonic freestream conditions are determined through a characteristic analysis normal to the boundary, including a point vortex representation for the induced velocities in the far field, similar to that described in Ref. 9. Along inflow boundaries for supersonic freestream conditions, quantities are extrapolated from the exterior; along outflow boundaries, quantities are extrapolated from the interior.

Baseline Computational Results

Computational results are shown in Figs. 4 and 5 for a baseline series of test cases. Comparisons are made between the Steger-Warming ($\epsilon = 0$) and the Van Leer flux splittings using MUSCL-type differencing with $\phi^{\pm} = 1$ (second-order spatial accuracy, no limiting). All of the results shown in Figs. 4 and 5 are for C-type grids with 161 grid points in the direction tangential to the airfoil and 41 grid points normal to the surface and wake. The grids extend approximately 12 chord lengths from the airfoil in all directions. Furthermore, each case was run using a variable time step throughout the grid based on a local CFL number. All cases ran 1000 iterations with a local CFL number of 30 specified everywhere (unless otherwise noted), starting from freestream conditions.

The first case considered is subcritical flow around an NACA 0012 airfoil at a freestream Mach number of $M_\infty = 0.63$ and an angle of attack $\alpha = 2$ deg. The distributions of pressure coefficients c_p are shown in Fig. 4a for the Van Leer and Steger-Warming flux splittings. Both solutions are nearly identical with a lift coefficient c_ℓ of 0.333 and 0.332, respectively, in close agreement with the value of 0.335 obtained by Lock[10] from an accurate solution based on the potential equation. The history of residual and lift obtained with Van Leer's flux splitting is shown in Fig. 5. The residual is defined as the L_2 norm of the right-hand side of Eq. (24) evaluated for the continuity equation only. The convergence rate indicates a spectral radius of approximately 0.978. The lift coefficient converges to its asymptotic value very rapidly, within 150-200 iterations. With the Steger-Warming flux splitting, the convergence was somewhat lower than that shown in Fig. 5 because of a reduction in the allowable CFL number.

The next case considered is supercritical flow over a NACA 0012 airfoil at $M_\infty = 0.80$ and $\alpha = 1.25$ deg. Under these conditions, a shock appears on both the upper and lower surfaces of the airfoil; the Mach number ahead of the

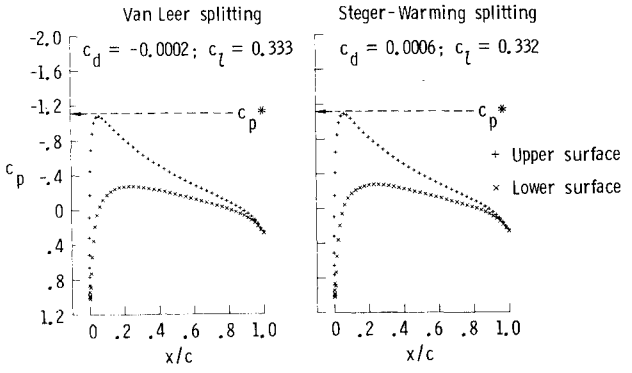

a) NACA 0012, $M_\infty = 0.63$, $\alpha = 2$ deg.

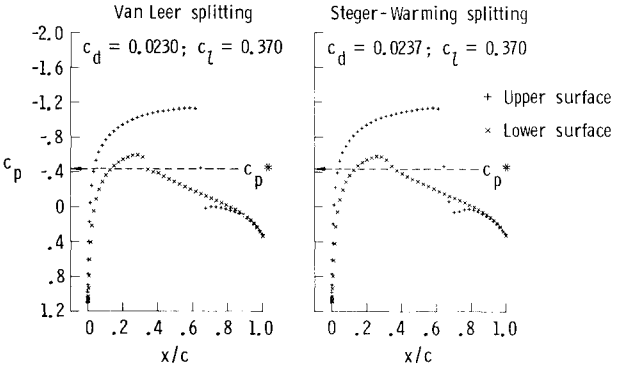

b) NACA 0012, $M_\infty = 0.80$, $\alpha = 1.25$ deg.

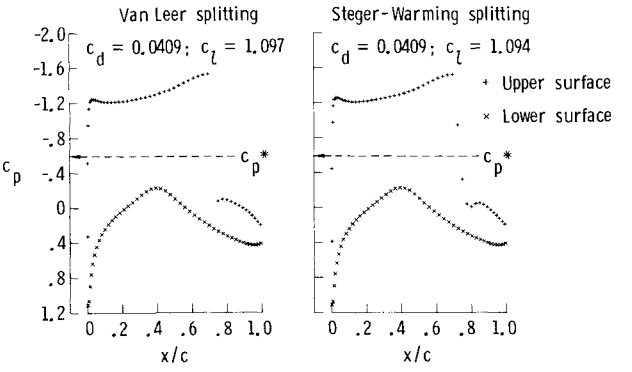

c) RAE 2822, $M_\infty = 0.75$, $\alpha = 3.00$ deg.

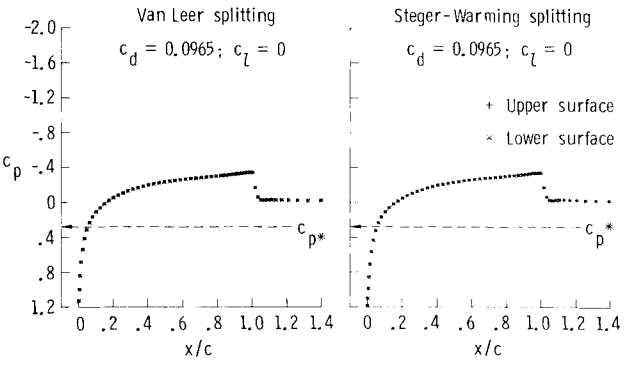

d) NACA 0012, $M_\infty = 1.2$, $\alpha = 0.0$ deg.

Fig. 4 Pressure distribution comparison between the Steger-Warming and Van Leer flux splittings (161 × 41 C-mesh).

upper shock is approximately 1.4. The residual and lift history is shown in Fig. 5 for the Van Leer splitting; the spectral radius of 0.976 for the transonic case is slightly better than for the subsonic case. The convergence rate with the Steger-Warming flux splitting was almost identical to that shown for the Van Leer splitting. A comparison between the pressure distributions of the Van Leer and Steger-Warming splittings in Fig. 4b shows that the Van Leer splitting leads to a sharper representation of both the upper and the lower shock, but neither solution exhibits undershoots or overshoots. This is the same qualitative behavior as seen in the one-dimensional test cases. The lift and drag coefficients, c_ℓ and c_d, obtained with the Van Leer splitting are 0.370 and 0.0230, respectively; with the Steger-Warming splitting, the lift is the same and the drag differs by only 3%.

Computations for the RAE 2822 airfoil at $M_\infty = 0.75$ and $\alpha = 3$ deg are shown in Figs. 4c and 5. The conditions correspond to a strong upper-surface shock with a Mach number ahead of the shock of about 1.5. The spectral radius for this case was 0.965; the residual was reduced to machine zero in less than 700 iterations, while the lift reached its final value in 125-150 iterations. The rate of convergence with the Steger-Warming splitting was less than that with the Van Leer splitting, due to a reduction in the allowable CFL number. As indicated in the pressure distributions in Fig. 4c, the Van Leer splitting leads to a sharper representation of the shock, although both solutions yield almost identical values for lift and drag. The lift and drag coefficients with the Van Leer splitting are 1.097 and 0.0409, respectively, while corresponding values of 1.094 and 0.0409 are obtained with the Steger-Warming splitting.

The last test case considered was an NACA 0012 airfoil at nonlifting, supersonic conditions: $M_\infty = 1.20$ and $\alpha = 0$ deg. Although not shown, the residual was reduced to machine zero in less than 300 iterations with the Van Leer splitting, corresponding to a spectral radius of 0.93; with the Steger-Warming splitting approximately 800 iterations were required because it was necessary to reduce the local CFL number to 10 in order to achieve convergence. The pressure distributions obtained with the two splittings are shown in Fig. 4d. The lift and drag coefficients for both splittings are zero and 0.0965, respectively. Both methods capture the oblique shock at the trailing edge very sharply. In this case, the streamwise flux differencing is identical in the majority of the cells, namely, in those cells with supersonic flow.

Extension to Third-Order Spatial Accuracy

The spatial differencing resulting from Eqs. (25-27) and applied above corresponds to a fully one-sided approximation of $\partial \hat{F}^{\pm}/\partial \xi$ and $\partial \hat{G}^{\pm}/\partial \eta$. By admitting an upwind-biased approximation, the accuracy can be increased to the third order. A general upwind-biased MUSCL-type scheme can be obtained by defining

$$Q^{-}_{i+\frac{1}{2},j} = Q_{i,j} + \tfrac{1}{4}\left[(1-\kappa)\Delta_- + (1+\kappa)\Delta_+\right]_{i,j} \tag{28}$$

$$Q^{+}_{i+\frac{1}{2},j} = Q_{i+1,j} - \tfrac{1}{4}\left[(1-\kappa)\Delta_+ + (1+\kappa)\Delta_-\right]_{i+1,j} \tag{29}$$

where

$$(\Delta_+)_{i,j} \equiv Q_{i+1,j} - Q_{i,j} \tag{30}$$

$$(\Delta_-)_{i,j} \equiv Q_{i,j} - Q_{i-1,j} \tag{31}$$

The fully one-sided approximation described earlier is obtained by inserting $\kappa = -1$ in the above equations. The value $\kappa = \frac{1}{3}$ leads to a third-order upwind-biased approximation, while $\kappa = +1$ yields the second-order central difference scheme. All upwind-biased approximations use the same number of cells for the residual computation as the fully one-sided approximation and may be implemented with only a slight increase in computational effort. It must be said that the third-order scheme is strictly third-order accurate only in one-dimensional calculations. To obtain a third-order scheme in two dimensions, it is not sufficient to compute the flux across a cell face on the basis of an averaged state. The difference between the averaged flux and the flux of the averaged state is a term of the second order and vanishes only for a linear system of conservation laws. Nevertheless, by switching from $k = -1$ to $\frac{1}{3}$, the accuracy of smooth solutions can be increased, as shown by Thomas and Walters[11]; in the present transonic solutions shown below, the differences are marginal.

In all computations with upwind-biased schemes, undershoots and overshoots in the shock region are expected. A limiter may be used to reduce the scheme to a fully one-sided scheme of either first- or second-order accuracy in the shock region, thus eliminating overshoots or undershoots. The first limiter chosen for this study is a so-called minimum-modulus (min-mod) limiter; it modifies the upwind-biased interpolations [Eqs. (28) and (29)] as follows:

$$Q^{-}_{i+\frac{1}{2},j} = Q_{i,j} + \tfrac{1}{4}\left[(1-\kappa)\bar{\Delta}_- + (1+\kappa)\bar{\Delta}_+\right]_{i,j} \tag{32}$$

$$Q^{+}_{i+\frac{1}{2},j} = Q_{i+1,j} - \tfrac{1}{4}\left[(1-\kappa)\bar{\Delta}_+ + (1+\kappa)\bar{\Delta}_-\right]_{i+1,j} \tag{33}$$

where

$$\bar{\Delta}_+ = \max\left[0, \min(\Delta_+ \operatorname{sgn}\Delta_-, b\Delta_- \operatorname{sgn}\Delta_+)\right]\operatorname{sgn}\Delta_+ \tag{34}$$

$$\bar{\Delta}_- = \max\left[0, \min(\Delta_- \operatorname{sgn}\Delta_+, b\Delta_+ \operatorname{sgn}\Delta_-)\right]\operatorname{sgn}\Delta_- \tag{35}$$

$$b = (3-\kappa)/(1-\kappa) \tag{36}$$

The residual history using this limiter often enters into a limit cycle oscillation as shown in Fig. 6 although the final

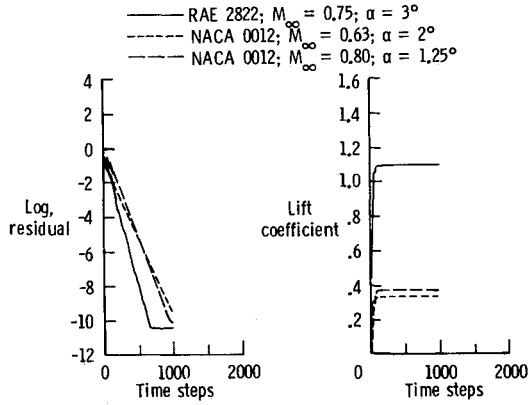

Fig. 5 Residual and lift histories with Van Leer splitting (161×41 C-mesh).

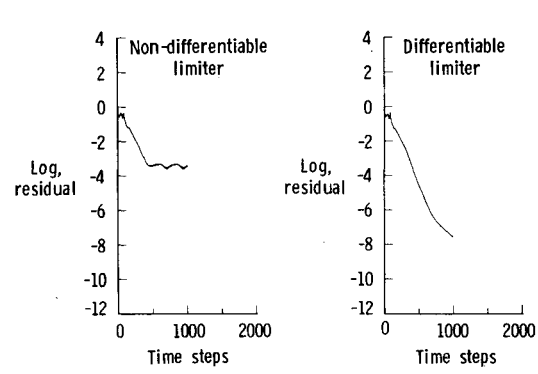

Fig. 6 Effect of limiting on residual history of NACA 0012, $M_\infty = 0.80$, $\alpha = 1.25$ deg (161×41 C-mesh).

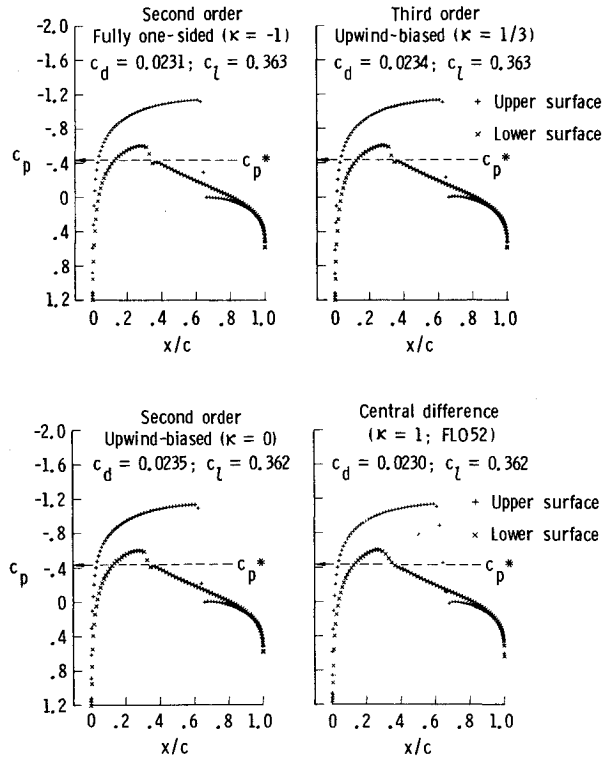

Fig. 7 Comparison of second and third-order accurate pressure distributions for NACA 0012 airfoil, $M_\infty = 0.80$, $\alpha = 1.25$ deg (161×41 O-mesh).

lift value is reached in approximately the same number of iterations as with the second-order scheme. The limit cycle is believed to be associated with the discontinuous derivative of the limiter in certain regions.

A second limiter, acting in a continuously differentiable manner,[6] was chosen in order to overcome the convergence problems encountered above. This limiter is implemented by rewriting Eqs. (28) and (29) as

$$Q^-_{i+\frac{1}{2},j} = Q_{i,j} + \{s/4[(1-\kappa s)\Delta_- + (1+\kappa s)\Delta_+]\}_{i,j} \quad (37)$$

$$Q^+_{i+\frac{1}{2},j} = Q_{i+1,j} - \{s/4[(1-\kappa s)\Delta_+ + (1+\kappa s)\Delta_-]\}_{i+1,j} \quad (38)$$

where

$$s = \frac{2\Delta_+\Delta_- + \epsilon}{(\Delta_+)^2 + (\Delta_-)^2 + \epsilon} \quad (39)$$

and ϵ is a small number ($\epsilon = 10^{-6}$) preventing division by zero in regions of null gradients. The residual using this limiter as shown in Fig. 6 decreases continuously, although not as fast as for the fully one-sided scheme. The pressure distribution obtained with the upwind-biased schemes agree closely with the fully one-sided scheme with no oscillations.

Finally, Fig. 7 shows a comparison of the present results for the one-sided ($\kappa = -1$) and upwind-biased (both $\kappa = 0$ and $\kappa = \frac{1}{3}$) schemes, with results from the central difference scheme developed by Jameson et al.[12] for the NACA 0012 airfoil at supercritical conditions. All results are obtained on the same mesh, which is of the O-type, with 160 cells around the airfoil and 40 cells in the direction normal to the airfoil. The three solutions yield similar pressure distributions over most of the airfoil, as well as similar values of lift and drag. The upwind approximations, however, give much sharper shock profiles than the central difference scheme, which particularly smears the lower surface shock. Further experiments with the central difference scheme indicate that the lower-surface shock can be resolved if much finer meshes are used.

Conclusions

An investigation has been conducted to compare the flux splitting method of Steger-Warming with that of Van Leer, including applications to quasi-one-dimensional transonic flow in a nozzle and two-dimensional subsonic, transonic, and supersonic flow over airfoils in generalized coordinates. The studies in one dimension indicate a definite advantage of the MUSCL approach (differencing followed by flux splitting) over the standard flux differencing approach (flux splitting followed by differencing). With the Steger-Warming splitting, for example, the approach allows a smooth transition from subsonic to supersonic flow without the need for extra smoothing. In addition, the fully one-sided MUSCL-type approach yields no over- or undershoots in the shock region when either the Van Leer or the Steger-Warming splitting is used. The Van Leer splitting leads to a sharper representation of shocks, with at most two zones (but generally one zone) in the shock transition.

A baseline series of computations of flow over two-dimensional airfoils ranging from subcritical lifting flow ($M_\infty = 0.63$) to supersonic nonlifting flow ($M_\infty = 1.2$) has been made. With an approximately factored implicit scheme and a fully one-sided second-order approximation to the flux derivatives incorporating the Van Leer splitting, the L_2 norm of the residual was reduced to machine zero in less than 1000 iterations for all cases on a 161×41 C-mesh. The spectral radius decreases from 0.978 for a subsonic case to 0.930 for a supersonic case. In all of the cases studied, the spectral radius decreases as a higher percentage of the flowfield becomes supersonic. With the Steger-Warming splittings, the rate of convergence is less, in general, because of a decrease in the allowable CFL number.

The second-order one-sided scheme is easily generalized to second- and third-order upwind-biased schemes, at little extra computational effort. These upwind-biased schemes, however, require a limiting of higher-order terms to avoid oscillations in the shock region. Two limiters have been tried, one of min-mod type, which is activated suddenly in regions of rapidly changing gradients, the other a smooth limiter with a continuous action. The mid-mod limiter caused a limit cycle in the residual on fine grids, whereas with the smooth limiter the solution continued to converge, although with a somewhat higher spectral radius than for the one-sided scheme. The pressure distributions for the one-sided second-order scheme as well as the upwind-biased third-order scheme both show sharp shocks and, in overall features, agree closely to results obtained with a widely used central-difference code. A weak shock arising on the lower airfoil surface in supercritical flow was resolved more accurately with the flux splitting approach than with the central difference approach.

References

[1]Steger, J. L. and Warming, R. F., "Flux Vector Splitting of the Inviscid Gasdynamic Equations with Application to Finite Difference Methods," *Journal of Computational Physics*, Vol. 40, No. 2, April 1981, pp. 263-293.

[2]Buning, P. G. and Steger, J. L., "Solution of the Two-Dimensional Euler Equations with Generalized Coordinate Transformation Using Flux Vector Splitting," AIAA Paper 82-0971, 1982.

[3]Van Leer, B., "Flux-Vector Splitting for the Euler Equations," ICASE Rept. 82-30, Sept. 1982 (also *Lecture Notes in Physics*, Vol. 170, 1982, pp. 507-512).

[4]Steger, J. L., "Preliminary Study of Relaxation Methods for the Inviscid Conservative Gasdynamics Equations Using Flux Splitting," NASA CR-3415, 1981.

[5]Van Leer, B., "Towards the Ultimate Conservative Difference Scheme V: A Second-Order Sequel to Gudonov's Method," *Journal of Computational Physics*, Vol. 32, 1979, pp. 101-136.

[6]Mulder, W. A. and Van Leer, B., "Implicit Upwind Methods for the Euler Equations," AIAA Paper 83-1930, July 1983.

[7]Beam, R. and Warming, R. F., "An Implicit Finite-Difference Algorithm for Hyperbolic Systems in Conservation-Law-Form," *Journal of Computational Physics*, Vol. 22, Sept. 1976, pp. 87-110.

[8]Jespersen, D. C. and Pulliam, T. H., "Flux Vector-Splitting and Approximate Newton Methods," AIAA Paper 83-1899, July 1983.

[9]Thomas, J. L. and Salas, M. D., "Far-Field Boundary Conditions for Transonic Lifting Solutions to the Euler Equations," AIAA Paper 85-0020, Jan. 1985.

[10]Lock, R. C., "Test Cases for Numerical Methods in Two-Dimensional Transonic Flows," AGARD Rept. 575, 1970.

[11]Thomas, J. L. and Walters, R. W., "Upwind Relaxation Algorithms for the Navier-Stokes Equations," AIAA Paper 85-1501, July 1985.

[12]Jameson, A., Schmidt, W., and Turkel, E., "Numerical Solutions of the Euler Equations by Finite Volume Methods Using Runge Kutta Time-Stepping Schemes," AIAA Paper 81-1259, June 1981.